Mechanical morphotype switching as an adaptive response in mycobacteria

Haig Alexander Eskandarian [1,4,*], Yu-Xiang Chen [1], Chiara Toniolo [2], Juan Belardinelli [3], Zuzana Palcekova [3], Paul Ashby [4,5], Georg E. Fantner [6], Mary Jackson [3], John D. McKinney [2], Babak Javid [1,*]

Affiliations:
[1] Division of Experimental Medicine, University of California San Francisco, San Francisco, CA, USA.
[2] School of Life Sciences, Swiss Federal Institute of Technology in Lausanne (EPFL), 1015 Lausanne, Switzerland.
[3] Mycobacteria Research Laboratories, Department of Microbiology, Immunology and Pathology, Colorado State University, Fort Collins, CO 80523-1682, USA.
[4] The Molecular Foundry, Lawrence Berkeley National Laboratory, Berkeley, CA 94720, USA.
[5] Materials Science Division, Lawrence Berkeley National Laboratory, Berkeley, CA 94720, USA.
[6] School of Engineering, Swiss Federal Institute of Technology (EPFL), 1015 Lausanne, Switzerland.
* e-mail: haig.eskandarian@ucsf.edu , babak.javid@ucsf.edu

Summary:

Bacterial stress tolerance during infection is commonly thought to be encoded by discrete biochemical stress-specific mechanisms [1]. However, increasing evidence suggests that fluctuating conditions of stress drive biomechanical changes to bacterial components on varying cellular scales [2-5]. Here, we use atomic-force microscopy (AFM) [6] to demonstrate that during macrophage infection, intracellular mycobacteria diverge into two mechanically distinct subpopulations exhibiting either a two-fold increase or decrease in mean cell surface stiffness. We describe this process as “mechanical morphotype switching”, which we define as a phenotypic differentiation into two distinct, semi-stable mechanical cell states. Mycobacterial mechanical morphotype states are enriched by gene mutation and cytokine modulation of host macrophage responses, suggesting a molecular basis for switching and a role for host immunity in driving selection of discrete mechanical morphotypes. Crucially, mycobacterial mechanical morphotype switching enhances survival in macrophages of both non-pathogenic *Mycobacterium smegmatis* and pathogenic, *M. abscessus*. These results reveal that mycobacteria mechanically adapt to enhance intracellular viability. Our study highlights the importance of bacterial mechanical properties for optimised survival in host intracellular environments during pathogenesis.

Results:

Atomic Force Microscopy has previously been used to characterise perturbations of cell wall components at the bacterial cell surface [3,7-9]. More recently, long-term time-lapse AFM (LTTL-AFM) on mycobacteria has defined a synergistic role for cell biomechanics and molecular components influencing fundamental cell processes, such as division site selection, cell cleavage and pole elongation [9-11]. Here, we used LTTL-AFM to dynamically characterise the distribution in mycobacterial cell surface mechanical properties during axenic growth, bacteriostatic and cidal stresses, and following macrophage infection (Figure 1a). Growth in *M. smegmatis* consists of pole elongation and subcellular changes in cell surface stiffness (Figure 1a & 1b, Supplementary Video 1, and Supplementary Figure S1). Elongation results from an expansion of cell volume by the addition of nascent cell wall material near the poles [9,10,12-14]. The elongating mycobacterial cell surface consists of three discrete regions of mechanically distinct material (Supplementary Figure S1). Most of the cell surface (~75%),

emanating from mid-cell and excluding the poles, is comprised of stably rigid cell surface material (Figure 1c, Supplemental Figures S1 & S2a). LTTL-AFM imaging reveals a process of "mechanical maturation", which we define as a zone of material localised nearest to the poles where nascent, non-crosslinked peptidoglycan is first deposited [14] and begins to stiffen (Figure 1c & Supplementary Figure S2a). Elongation at the old pole shifts the mechanically rigid zone towards the new-pole daughter in the lag-phase, which precedes new-end take-off (NETO) at the new pole [10]. Mechanical maturation spans ~25% of the cell length (~20% at the old pole and 7% at new pole, pre-NETO) (Figure 1c, Supplementary Figure S2a) and corresponds to the previously reported sub-cellular zones where nascent non-crosslinked cell wall material is localised [14,15].

The mycobacterial cell wall is composed of multiple layers believed to mechanically maintain cell morphology as load-bearing units [16,17]. Mutant cells exhibiting defective peptidoglycan crosslinking by the knockout of L,D–transpeptidases (Δ*ldtAEBCG+F*) results in a two-fold decrease in mean cell surface stiffness [14] culminating in a gradually expanding bulge near the new pole (Supplementary Video 2). In contrast, inhibiting proteins involved in the maturation and export of arabinogalactan and lipoarabinomannan (Δ*Rv1410-lprG* and Δ*sucT*) results in increased mean cell surface stiffness [18-21]. Dynamic shifts in *M. smegmatis* cell surface stiffness was defined using biochemical perturbation of cell wall biogenesis. Mycobacteria treated with isoniazid (INH) causes a gradual two-fold increase in mean cell surface stiffness and collapsed phenotypic heterogeneity (Supplementary Figure S3a). The zones of mechanically distinct cell surface material were abolished by INH-induced reductive division and arrest of pole elongation (Supplementary Figure S2b). Recovery of ~60% of *M. smegmatis* cells from INH-treatment entailed a resumption of pole elongation resulting in the addition of nascent material undergoing a gradual mechanical maturation to untreated levels (Supplementary Figure S3a & S4, Supplementary Video 3). Treatment with the bacteriostatic cyanide derivative, Carbonyl cyanide m-chlorophenyl hydrazone (CCCP), caused a rapid ~35% decrease in mean cell surface stiffness (10 kPa min^{-1}), which was partially reversed by exchanging the tonicity of the growth medium with deionised water (Supplementary Figure S3b). Release from CCCP treatment results in a gradual recovery of mean cell surface stiffness (~5 kPa min^{-1}) and is concomitant with a recovery of nearly all treated bacilli (Supplementary Figure 4). *M. smegmatis* cells released from CCCP-treatment begin to

recover their mean cell surface stiffness prior to the resumption of elongation (Supplementary Video 4).

Macrophages represent an important host cell niche for mycobacterial pathogens [22]. We used intracellular macrophage stress to understand the selection of discrete mechanical morphotype states (Figure 2a). *M. smegmatis* recovered following infection of bone marrow-derived macrophages (BMDMs) exhibited divergent selection into two mechanically differentiated phenotypic states (Figure 2b). Macrophage selection resulted in the recovery of bacilli exhibiting predominantly decreased cell surface stiffness (Figure 2b & 2c). Heterogeneity in cell lengths increased over the course of the infection among mechanically "soft" bacilli (Supplementary Figure S5). Mechanically "soft" bacilli exhibited elongated chains of un-cleaved daughter cells reminiscent of hydrolase defective mutants [9,11,23], though with two spatially proximal pre-cleavage furrows (Figure 2b). Cytokine stimulation of macrophages represents a critical axis by which to control infection and reflects a discrete state of immune activation [24]. Macrophage stimulation with interferon gamma (IFNγ) resulted in the emergence of mechanically "hard" bacilli (Figure 2d). To expand the study of mechanical properties in larger bacterial populations, AFM results were corroborated using buoyancy centrifugation as a surrogate strategy. Samples were fractionated into three buoyancy states, recovering bacilli in "low" (<1.064 g cm^{-3}), "middle" (between 1.064 – 1.102 g cm^{-3}), and "high" (>1.102 g cm^{-3}) fractions, based on reported limits in the fractionation of mycobacterial cultures by buoyancy centrifugation [25]. Increased bacterial surface stiffness correlated to individuals recovered from a "high" buoyancy fraction and mechanically "soft" bacilli were recovered from a low buoyancy fraction (Supplementary Figure 6). *M. smegmatis* isolated from unstimulated macrophages was predominantly recovered from a "low" buoyancy fraction and bacilli isolated from IFNγ-stimulated macrophages were principally recovered from a "high" buoyancy fraction (Supplementary Figure 7a-c). Optical fluorescence microscopy (OFM) revealed that acidification of mycobacteria-containing vacuoles was ubiquitous in both untreated and cytokine-stimulated macrophages (Supplementary Figure 8). Intracellular *M. smegmatis* isolated from IFNγ-stimulated macrophages treated with bafilomycin A, an inhibitor of vacuolar maturation, caused reversion of the mechanical morphotype to a "low" buoyancy cell state (Supplementary Figure 9), supporting a role for phagosomal maturation in the selection of the "hard" mechanical morphotype.

The physiological consequence of mycobacterial differentiation into two distinct mechanical cell states was evaluated by quantifying the rate of regrowth of individual bacilli representing each discrete mechanical morphotype (Figure 3a). Intracellular mycobacteria were isolated from lysed macrophages, fractionated by buoyancy centrifugation (Figure 3a) and the relative recovery rate quantified using LTTL-AFM or plated colony forming units (cfu). The rate of regrowth for "soft" bacilli was two-fold higher than the "hard" in unstimulated macrophages and three-fold in IFNγ-stimulated macrophages (Figure 3b). Using colony forming units to quantify relative recovery of "low" versus "high" buoyancy fractions, the "low" buoyancy fraction exhibited ten-fold greater recovery than the "high" buoyancy fraction in unstimulated macrophages and a two-fold difference in interferon-stimulated macrophages (Figure 3c).

These results present the possibility that there exists an order of switching from one semi-stable mechanical morphotype to another. We hypothesized that mutants locking *M. smegmatis* into a specific mechanical morphotype state could be isolated with appropriate selection. High density transposon-mutagenised libraries in *M. smegmatis* [26] were sorted by buoyancy fractionation to identify genes required for regulating the maintenance of a mechanical morphotype state (low buoyancy) or "hard" (high buoyancy) state (Supplementary Figure 6a). Transposon insertion site frequencies were mapped by deep sequencing and compared with the unfractionated input library. Gene essentiality of transposon mutants was identified in the absence of transposon insertions found in a "low" (soft) or "high" (hard) buoyancy fraction. These likely corresponded to mutants for which the capacity to switch out of a "soft" or "hard" mechanical morphotype was compromised, resulting in enrichment of the morphotype. We identified a restrictive group of genes regulating the "low" buoyancy mechanical morphotype (Figure 4a). None of the hits identified following the stringent post-hoc correction were among highly conserved genes. Since we wanted to extend our findings to other mycobacteria, we asked whether relaxing the post-hoc correction would enable us to identify conserved genes among the mechanical morphotype mutants. By relaxing post-hoc correction, we identified many more mutants that appeared to be locked into a "low" buoyancy fraction. By contrast, very few mutants were identified that were locked into a "high" buoyancy fraction (Figure 4b & 4c). The top candidate identified among the "low" buoyancy mechano-morphotype mutants was Δ*Ms3378*, a predicted beta-lactamase (Figure 4a). Another candidate gene identified in our screen, *uvrA*, is characterised as an essential member of the

uvrABC gene system responsible for DNA damage repair and widely conserved in bacteria [27,28] (Figure 4b). The *uvrABC* system was previously reported to enhance mycobacterial persistence to host intracellular stresses [29] though is equally reported to decrease in expression over the course of infection [30]. Using AFM to quantify the mean cell surface stiffness of both Δ*Ms3378* and Δ*uvrA*, showed that both exhibited decreased cell surface stiffness as compared to WT *M. smegmatis* (Figure 4d), confirming the validity of our screening approach. Buoyancy fractionation of mechano-morphotype mutant candidate Δ*Ms3378* isolated from axenic growth conditions revealed an equivalent relative recovery rate in "middle" and "low" buoyancy fractions whereas Δ*uvrA* was isolated predominantly from a "low" buoyancy fraction (Supplementary Figure 10a & 10b).

Due to the lack of an AFM in biosafety containment, buoyancy fractionation enabled us to evaluate the generalisability of mechanical morphotype switching by interrogating the distribution in mechanical cell states of *M. abscessus*, a non-tuberculous mycobacterium (NTM) and pathogen. *M. abscessus* cultured in axenic conditions of growth was recovered from the "low" buoyancy fraction (Supplementary Figure 7d), representing a significant shift towards "low" buoyancy as compared to *M. smegmatis*. Both smooth and rough colony morphology variants [31] exhibited similar fractional distributions in buoyancy (Supplementary Figure 7g & 7h). *M. abscessus* recovered from macrophages exhibited the same distributions in buoyancy fractionation as *M. smegmatis*, that is, a "low" buoyancy fraction predominated in unstimulated macrophages and a "high" buoyancy fraction in IFNγ-stimulated macrophages (Supplementary Figure 7e & 7f), supporting the generalisability of our findings to both non-pathogenic and pathogenic mycobacteria.

Having failed to identify transposon mutants representing conserved genes in the high buoyancy fraction, we chose *sucT* to evaluate mechanical morphotype switching of a mutant representing a "hard" cell state, a mutant previously characterised to exhibit a 2-fold increase in cell surface stiffness [19]. We confirmed that the mutants Δ*uvrA* and Δ*sucT* had similar phenotypes in *M. smegmatis* and *M. abscessus*. Buoyancy fractionation of *Ms*Δ*sucT* revealed that bacteria were predominantly isolated from a "high" buoyancy fraction, while *sucT* complementation in *M. smegmatis* reverted to the distribution of mechanical properties exhibited by WT (Supplementary Figure 11). *sucT* complementation in *M. smegmatis* equally recapitulated mechanical morphotype switching exhibited by wildtype *M. smegmatis* in

macrophages (Supplementary Figure 11d & 11e). *Mab*Δ*uvrA* was predominantly isolated from a "low" buoyancy fraction while *Mab*Δ*sucT* was predominantly isolated from a "high" buoyancy fraction when cultured in axenic conditions of growth (Supplementary Figure 12), recapitulating the observations in *M. smegmatis* that these genes influence the mechanical state of the cell. *Mab*Δ*uvrA* was equally enriched in a "low" buoyancy cell state when isolated from both unstimulated and IFNγ-stimulated macrophages (Supplementary Figure 13). *Mab*Δ*sucT* was recovered predominantly from a "high" buoyancy fraction in both unstimulated and IFNγ-stimulated macrophages (Supplementary Figure 13).

We sought to investigate whether mechanical morphotype switching provides an adaptive advantage in tolerating macrophage infection. The "soft" mechano-morphotype mutants, *Ms*Δ*uvrA* and Δ*Ms3378*, both had increased fractional recovery when isolated from macrophages, particularly in IFNγ-stimulated macrophages with a ~6-fold and >20-fold increase, respectively, as compared to wildtype (Figure 4e). Fractional recovery of *Ms*Δ*sucT* was attenuated as compared to wildtype in both unstimulated and IFNγ-stimulated macrophages (Figure 4e). Similarly, *Mab*Δ*uvrA* isolated from unstimulated macrophages exhibited 20% increased recovery as compared to wildtype and a >5-fold increase upon IFNγ-stimulation (Figure 4f). *Mab*Δ*sucT* exhibited a two-fold decreased survival during infection of unstimulated macrophages as compared to wildtype, a host cell condition selecting for the predominance of a "soft" mechanical cell state (Figure 4f). In IFNγ-stimulated macrophages, which drives selection of a "hard" mechanical cell state (Supplementary Figure 7f), wildtype *Mab* and *Mab*Δ*sucT* exhibited similar rates of recovery (Figure 4f).

Our findings fundamentally expand the understanding of how mycobacteria modulate cell surface mechanical properties to become refractory to killing in emerging conditions of stress. Previous studies outline limits in the mechanical variation of bacterial cell wall integrity and cytosolic tonicity [3,5,25,32,33], both of which are fundamental cell properties that can influence the impact of bactericidal stress. We show that *M. smegmatis* and *M. abscessus* undergo cell mechanical differentiation emerging as distinct, semi-stable cell states. What might be the biophysical nature of mechanical morphotype switching? Two principal cell mechanical properties might work in conjunction with one another to drive mechanical morphotype switching. The architecture of the cell wall plays a major role in setting the pattern of mechanically distinct growth zones and thinning of outer cell wall layers results in increased

cell surface stiffness [18,19]. Concomitant with shifts in cell surface stiffness are changes in buoyant density, which can be modulated by changes in cytosolic tonicity [3,14]. Cytosolic tonicity influences turgor pressure, which is a major force pushing outward against the mycobacterial cell wall and generating the stiffness at the cell surface [11]. Decreased turgor pressure might explain why "soft" mechanical morphotype bacilli isolated from unstimulated macrophages appear as elongated, chained cells exhibiting double septa, as this force was previously shown to drive cleavage of daughter cells in *M. smegmatis* [11].

How might mechanical morphotype switching be controlled? The rate of mechanical morphotype switching might provide insights into which mechanical cell properties influence the trajectory of switching. The gradual switch of *M. smegmatis* to a "hard" mechanical morphotype state upon treatment with isoniazid (Supplementary Figure 3) contrasts with the rapid switch to a "soft" mechanical morphotype state upon treatment with CCCP (Supplementary Figure 4). Mechanical properties acting on different timescales might provide insight into the logical trajectory of switching. A bulging deformation in the Δ*ldtAEBCG+F* mutant occurs gradually as a function of growth in static isotonic conditions (Supplementary Video 2), suggesting that cell wall architectural change occurs on slow timescales comparable to a switch to a "hard" mechanical morphotype state. By contrast, mechanical forces functioning on rapid timescales might influence the rapid rate at which bacteria switch into a "soft" mechanical morphotype state. A decrease in cytosolic tonicity in mycobacteria [14] might account for the rapid switch to the "soft" mechanical morphotype state. In the gram-negative *Escherichia coli*, rapid hyperosmotic shocks reduce turgor pressure, driving buckling of the inner cell membrane (plasmolysis) and decreases in cell surface stiffness [3].

Our transposon screen revealed functionally diverse mycobacterial genes mediating switching out of a mechanically "soft" cell state, suggesting that these functionally disparate genes buffer the "softening" of a population and define the lower limit of cell mechanical phenotypic heterogeneity. These observations might suggest that mycobacterial cells constitutively switch into (and out of) a "soft" morphotypic state and require negative regulation to enrich the soft morphotype. One key modulator identified to influence the enrichment of a "soft" mechanical morphotype, *uvrA*, is reported to gradually decrease in gene expression during macrophage infection by *M. tuberculosis* [30]. Remarkably, switching to a "soft" mechanical morphotype state

enhances survival in macrophages in both the non-pathogenic, *M. smegmatis*, and the pathogen, *M. abscessus*.

Interferon-dependent host vacuolar maturation is necessary to provoke a switch to the "hard" mechanical morphotype. It is possible that vacuolar maturation, which has the potential to control macrophage infection by mycobacterial pathogens [34], may impose a selective pressure favoring a less adapted "hard" mechanical morphotype state and represents a host response to curtail adaptive microbial biomechanical phenotypes. A "hardened" cell surface correlates with an increase in buoyancy and increased cytosolic accumulation of Calcein-AM [18]. An osmosensory system controlled by sigF and eukaryotic-like Ser/Thr protein kinase receptor, PknD, was reported in *M. tuberculosis* to remodel the cell wall and optimise cytosolic tonicity [35]; this might represent a morphogenetic program functioning as an adaptive response to cytokine-induced macrophage stress.

Here we present evidence that mechanical morphotype switching in mycobacteria to a "soft" state represents an adaptive response to host stress resulting in enhanced survival. Our identification of molecular regulators suggests that mechanical morphotype switching might represent a general mechanism harnessed by bacteria to respond generally to unpredictable fluctuating environmental conditions of stress. That mycobacteria possess the capacity to mechanically switch to both "hard" and "soft" cell states highlights the need for bacilli to respond to diverse host cell stress conditions. The "hard" mechanical morphotype might represent a selectively adapted cell state in permissive, hypo-osmotic environmental conditions. The finding that "soft" mechanical morphotype mutants represents an adaptive cell state exhibiting enhanced intracellular survival in macrophages provides a platform for the development of novel antimicrobial therapeutic compounds targeting the principle of mechanical adaptation.

Author Contributions:

HAE, YC, CT, and BJ conceived of experiments. CT and HAE conducted macrophage infections and optical fluorescence microscopy. YC and HAE conducted transposon mutagenesis and YC analysed TnSeq data. JB produced and provided knockout mutants in *Msm* and *Mab*. PA provided access to AFM system at LBNL. HAE conducted AFM imaging, image processing, and data analyses. JB, ZP, and MJ provided genetic mutants in *Msm* and *Mab*. JDM provided funds and infrastructure at EPFL. BJ provided funds and infrastructure at UCSF. HAE and BJ organised, wrote, and edited manuscript. HAE, YC, CT, BJ, ZP, PA, MJ, JDM and BJ all provided critical edits to the manuscript.

Acknowledgements:

HAE was supported by EMBO LTF, aLTF fellowships and funds provided by the JDM lab while at EPFL; by funds provided by the BJ lab and a Cystic Fibrosis Pilot and Feasibility Award (#002510I221 to HAE) at UCSF, and rapid and standard access proposals with affiliate status at the Molecular Foundry, at Lawrence Berkeley National Laboratory. CT was supported by funding from the European Union's Horizon 2020 research and innovation program under the Marie Skłodowska-Curie grant agreement No. 665667 at EPFL. This work was supported in part by a research grant from the Cystic Fibrosis Foundation (#JACKSO21G0 to MJ), and the National Institutes of Health/ National Institute of Allergy and Infectious Diseases grants AI155674 and AI167204 (to MJ). JMB is the recipient of a Vertex Research Innovation Award. BJ is a Wellcome Trust Investigator (207487/C/17/Z).

References:

1 Balaban, N. Q. *et al.* Definitions and guidelines for research on antibiotic persistence. *Nat Rev Microbiol* **17**, 441-448, doi:10.1038/s41579-019-0196-3 (2019).

2 Moyed, H. S. & Bertrand, K. P. hipA, a newly recognized gene of Escherichia coli K-12 that affects frequency of persistence after inhibition of murein synthesis. *J Bacteriol* **155**, 768-775, doi:10.1128/JB.155.2.768-775.1983 (1983).

3 Rojas, E. R. *et al.* The outer membrane is an essential load-bearing element in Gram-negative bacteria. *Nature* **559**, 617-621, doi:10.1038/s41586-018-0344-3 (2018).

4 Johansson, J. *et al.* An RNA thermosensor controls expression of virulence genes in Listeria monocytogenes. *Cell* **110**, 551-561, doi:10.1016/s0092-8674(02)00905-4 (2002).

5 Hakansson, S., Granlund-Edstedt, M., Sellin, M. & Holm, S. E. Demonstration and characterization of buoyant-density subpopulations of group B Streptococcus type III. *J Infect Dis* **161**, 741-746, doi:10.1093/infdis/161.4.741 (1990).

6 Eskandarian, H. A., Nievergelt, A. P. & Fantner, G. E. Time-Resolved Imaging of Bacterial Surfaces Using Atomic Force Microscopy. *Methods Mol Biol* **1814**, 385-402, doi:10.1007/978-1-4939-8591-3_23 (2018).

7 Fantner, G. E., Barbero, R. J., Gray, D. S. & Belcher, A. M. Kinetics of antimicrobial peptide activity measured on individual bacterial cells using high-speed atomic force microscopy. *Nat Nanotechnol* **5**, 280-285, doi:10.1038/nnano.2010.29 (2010).

8 Viljoen, A., Rath, E., McKinney, J. D., Fantner, G. E. & Dufrene, Y. F. Seeing and Touching the Mycomembrane at the Nanoscale. *J Bacteriol* **203**, doi:10.1128/JB.00547-20 (2021).

9 Eskandarian, H. A. *et al.* Division site selection linked to inherited cell surface wave troughs in mycobacteria. *Nat Microbiol* **2**, 17094, doi:10.1038/nmicrobiol.2017.94 (2017).

10 Hannebelle, M. T. M. *et al.* A biphasic growth model for cell pole elongation in mycobacteria. *Nat Commun* **11**, 452, doi:10.1038/s41467-019-14088-z (2020).

11 Odermatt, P. D. *et al.* Overlapping and essential roles for molecular and mechanical mechanisms in mycobacterial cell division. *Nat Phys* **16**, 57-62, doi:10.1038/s41567-019-0679-1 (2020).

12 Aldridge, B. B. *et al.* Asymmetry and aging of mycobacterial cells lead to variable growth and antibiotic susceptibility. *Science* **335**, 100-104, doi:10.1126/science.1216166 (2012).

13 Wakamoto, Y. *et al.* Dynamic persistence of antibiotic-stressed mycobacteria. *Science* **339**, 91-95, doi:10.1126/science.1229858 (2013).

14 Baranowski, C. *et al.* Maturing Mycobacterium smegmatis peptidoglycan requires non-canonical crosslinks to maintain shape. *Elife* **7**, doi:10.7554/eLife.37516 (2018).

15 Rodriguez-Rivera, F. P., Zhou, X., Theriot, J. A. & Bertozzi, C. R. Acute Modulation of Mycobacterial Cell Envelope Biogenesis by Front-Line Tuberculosis Drugs. *Angew Chem Int Ed Engl* **57**, 5267-5272, doi:10.1002/anie.201712020 (2018).

16 Alderwick, L. J., Harrison, J., Lloyd, G. S. & Birch, H. L. The Mycobacterial Cell Wall--Peptidoglycan and Arabinogalactan. *Cold Spring Harb Perspect Med* **5**, a021113, doi:10.1101/cshperspect.a021113 (2015).

17 Hett, E. C. & Rubin, E. J. Bacterial growth and cell division: a mycobacterial perspective. *Microbiol Mol Biol Rev* **72**, 126-156, table of contents, doi:10.1128/MMBR.00028-07 (2008).

18 Hohl, M. *et al.* Increased drug permeability of a stiffened mycobacterial outer membrane in cells lacking MFS transporter Rv1410 and lipoprotein LprG. *Mol Microbiol* **111**, 1263-1282, doi:10.1111/mmi.14220 (2019).

19 Palcekova, Z. *et al.* Disruption of the SucT acyltransferase in Mycobacterium smegmatis abrogates succinylation of cell envelope polysaccharides. *J Biol Chem* **294**, 10325-10335, doi:10.1074/jbc.RA119.008585 (2019).

20 Gaur, R. L. *et al.* LprG-mediated surface expression of lipoarabinomannan is essential for virulence of Mycobacterium tuberculosis. *PLoS Pathog* **10**, e1004376, doi:10.1371/journal.ppat.1004376 (2014).

21 Shukla, S. *et al.* Mycobacterium tuberculosis lipoprotein LprG binds lipoarabinomannan and determines its cell envelope localization to control phagolysosomal fusion. *PLoS Pathog* **10**, e1004471, doi:10.1371/journal.ppat.1004471 (2014).

22 Cohen, S. B. *et al.* Alveolar Macrophages Provide an Early Mycobacterium tuberculosis Niche and Initiate Dissemination. *Cell Host Microbe* **24**, 439-446 e434, doi:10.1016/j.chom.2018.08.001 (2018).

23 Hett, E. C., Chao, M. C., Deng, L. L. & Rubin, E. J. A mycobacterial enzyme essential for cell division synergizes with resuscitation-promoting factor. *PLoS Pathog* **4**, e1000001, doi:10.1371/journal.ppat.1000001 (2008).

24 Domingo-Gonzalez, R., Prince, O., Cooper, A. & Khader, S. A. Cytokines and Chemokines in Mycobacterium tuberculosis Infection. *Microbiol Spectr* **4**, doi:10.1128/microbiolspec.TBTB2-0018-2016 (2016).

25 den Hertog, A. L., Klatser, P. R. & Anthony, R. M. Buoyant density of Mycobacterium tuberculosis: implications for sputum processing. *Int J Tuberc Lung Dis* **13**, 466-471 (2009).

26 DeJesus, M. A., Ambadipudi, C., Baker, R., Sassetti, C. & Ioerger, T. R. TRANSIT--A Software Tool for Himar1 TnSeq Analysis. *PLoS Comput Biol* **11**, e1004401, doi:10.1371/journal.pcbi.1004401 (2015).

27 Truglio, J. J., Croteau, D. L., Van Houten, B. & Kisker, C. Prokaryotic nucleotide excision repair: the UvrABC system. *Chem Rev* **106**, 233-252, doi:10.1021/cr040471u (2006).

28 Van Houten, B., Croteau, D. L., DellaVecchia, M. J., Wang, H. & Kisker, C. 'Close-fitting sleeves': DNA damage recognition by the UvrABC nuclease system. *Mutat Res* **577**, 92-117, doi:10.1016/j.mrfmmm.2005.03.013 (2005).

29 Mazloum, N. *et al.* Identification of a chemical that inhibits the mycobacterial UvrABC complex in nucleotide excision repair. *Biochemistry* **50**, 1329-1335, doi:10.1021/bi101674c (2011).

30 Graham, J. E. & Clark-Curtiss, J. E. Identification of Mycobacterium tuberculosis RNAs synthesized in response to phagocytosis by human macrophages by selective capture of transcribed sequences (SCOTS). *Proc Natl Acad Sci U S A* **96**, 11554-11559, doi:10.1073/pnas.96.20.11554 (1999).

31 Howard, S. T. *et al.* Spontaneous reversion of Mycobacterium abscessus from a smooth to a rough morphotype is associated with reduced expression of glycopeptidolipid and reacquisition of an invasive phenotype. *Microbiology (Reading)* **152**, 1581-1590, doi:10.1099/mic.0.28625-0 (2006).

32 Auer, G. K. *et al.* Mechanical Genomics Identifies Diverse Modulators of Bacterial Cell Stiffness. *Cell Syst* **2**, 402-411, doi:10.1016/j.cels.2016.05.006 (2016).

33 Parry, B. R. *et al.* The bacterial cytoplasm has glass-like properties and is fluidized by metabolic activity. *Cell* **156**, 183-194, doi:10.1016/j.cell.2013.11.028 (2014).

34 Kimmey, J. M. *et al.* Unique role for ATG5 in neutrophil-mediated immunopathology during M. tuberculosis infection. *Nature* **528**, 565-569, doi:10.1038/nature16451 (2015).

35 Hatzios, S. K. *et al.* Osmosensory signaling in Mycobacterium tuberculosis mediated by a eukaryotic-like Ser/Thr protein kinase. *Proc Natl Acad Sci U S A* **110**, E5069-5077, doi:10.1073/pnas.1321205110 (2013).

36 Murphy, K. C. *et al.* ORBIT: a New Paradigm for Genetic Engineering of Mycobacterial Chromosomes. *mBio* **9**, doi:10.1128/mBio.01467-18 (2018).

37 Odermatt, P. D. *et al.* High-Resolution Correlative Microscopy: Bridging the Gap between Single Molecule Localization Microscopy and Atomic Force Microscopy. *Nano Lett* **15**, 4896-4904, doi:10.1021/acs.nanolett.5b00572 (2015).

38 Rodriguez-Rivera, F. P., Zhou, X., Theriot, J. A. & Bertozzi, C. R. Visualization of mycobacterial membrane dynamics in live cells. *J Am Chem Soc* **139**, 3488-3495, doi:10.1021/jacs.6b12541 (2017).

39 Santi, I., Dhar, N., Bousbaine, D., Wakamoto, Y. & McKinney, J. D. Single-cell dynamics of the chromosome replication and cell division cycles in mycobacteria. *Nat Commun* **4**, 2470, doi:10.1038/ncomms3470 (2013).

Methods:

Bacteria.

Mycobacterium smegmatis mc^{2}155 (wild-type) and derivative strains and *Mycobacterium abscessus* (ATCC 19977) and derivative strains were grown in Middlebrook 7H9 liquid medium (Difco) supplemented with 0.5% albumin, 0.2% glucose, 0.085% NaCl, 0.5% glycerol, and 0.5% Tween-80. Cultures were grown at 37°C to mid-exponential phase (optical density at 600nm (OD_{600}) of ~0.5). Aliquots were stored in 15% glycerol at -80°C and thawed at room temperature before use. The Δ*uvrA* strains were made by allelic exchange with an unmarked in-frame deletion of the *uvrA* gene in both *M. smegmatis* and *M. abscessus*. The *attB*-integrating plasmid expressing a *uvrA-wasabi* fusion was used to complement the gene *uvrA* into the *Ms*Δ*uvrA* strain. Construction of the *M. smegmatis sucT* complementation strain was described previously [19]. Chemico-mechanical manipulation of mycobacteria was conducted by treatments with isoniazid (INH) (Sigma) at 10 µg/ml^{-1} (2x minimum inhibitory concentration (MIC)) or 5 µM carbonyl cyanide-m-chlorophenylhydrazone (CCCP).

M. abscessus ATCC 19977 *uvrA* KO.

Deletion of *uvrA* (*MAB_2315*) from *M. abscessus* ATCC 19977 was carried out using the ORBIT system described by Murphy, *et al.* [36]. Briefly, *M. abscessus* was transformed with plasmid pKM444 expressing the Che9c phage RecT annealase and the Bxb1 phage integrase under control of the inducible pTet promoter. A 20ml culture of *Mabs* pKM444 as grown at 37C until OD=0.5, anhydrotetracycline was added at a final concentration of 500ng/ml to induce expression and cells were further incubated for 4h until OD=1. At this point, cells were harvested, washed 3 times with 10% glycerol and resuspended in 2ml of 10% glycerol. An aliquot of 380ml of cells was co-transformed with 200ng of payload plasmid pKM496 (Zeo^R) plus 1mg of ORBIT oligo and incubated O/N with shaking at 37°C to let them recover. Cells were collected and spread on 7H11 ADC + Zeo (100mg/ml); plates were incubated for 5 days at 37°C and colonies were picked and checked by PCR to verify the recombinants.

Transposon library construction, genomic DNA Extraction, and sequencing.

Transposon library after buoyancy centrifugation was collected and resuspended in 400ul 10mM Tris (pH=9). After beads-beating, genomic DNA was extracted by Phenol-Chloroform method. DNA concentration was measured and quantified by Nanodrop and Qubit. For building transposon sequencing library, approximately 5ug genomic DNA was resuspended in 150ul TE buffer and transferred to a Covaris tube, Genomic DNA was disrupted to 200-500bp size range by sonication with the following parameters: duty cycle (10%), intensity (4), cycles/burst (200), time (80s). The fragmented genomic DNA was size-selected and purified by AMPure XP beads. The fragmented genomic DNA was further subjected to end repair and dA tailing. Annealed adapter was ligated to the dA tailed fragmented genomic DNA and the linked ligated DNA fragment was used as template of 1st round nested PCR to amplify fragments containing adaptor and transposon junction. Indexed barcoded sequencing and illumina sequencing adaptor was added by 2nd nested PCR. All sequence libraries were examined by Agilent 2100 Bioanalyzer and subjected to next generation sequencing.

Transposon mutagenesis.

Mycobacterium smegmatis mc^{2}155 strain was grown to stationary phase (OD>6) in 50ml of 7H9 growth medium. Bacterial cultures were washed and resuspended in 5ml MP buffer (50mM Tris, 150mM NaCl,

10mM MgSO4, 2mM CaCl2). To transduce bacteria with MycoMarT7 phage, approximately 10^{11} plaque forming units of phage (PFU) was added to the bacterial suspension in MP buffer and incubated at 37°C for 4h. Immediately after transduction, ~300-400ul of the transduction mixture was plated on 15-cm LB agar plates, containing 20ug/ml kanamycin and 0.1% Tween80. After 3 days, library size was determined, and bacteria was scrapped and stored in 7h9 medium plus 15% glycerol as library stock. The transposon library was made in triplicate. The transposon library was cultured to an OD_{600nm} of 0.8 and 1ml of sample was loaded onto 10ml of stock isotonic percoll medium, with buoyant density beads as fiducial markers. Buoyancy centrifugation was conducted at 18°C, and spinning at 20k rpm (~50,000 g), for 1h20m. Three buoyancy fractions were isolated: "high" (>1.02 g cm^{-3}, <1.064 g cm^{-3}), "middle" (>1.064 g cm^{-3}, <1.102 g cm^{-3}), and "low" (>1.102 g cm^{-3}). Three biological replicates of the buoyancy centrifugation were conducted for the transposon library made in triplicate each of the three transposon libraries: 3 (libraries) x 3 (buoyancy centrifugation experiments) x 3 (buoyancy fractions) = 27 individual samples.

Transposon mapping and analysis.

Reads processing and TA loci mapping were performed through software TRANSIT [26]. Loci that were differentially disrupted by transposon were analysed using resampling test in TRANSIT with default parameter. Different buoyancy fractions were compared with input libraries and genes that are over-represented (log2FC < -1, adjusted p-value < 0.05) and under-represented (Log2FC >1, p-value < 0.05) were plotted.

ORBIT oligo for uvrA KO.

CGGTTCACCAACGGCGGCGTCAGTCATGACTGCCACCCTAGACCGGAGTGACAACCTTCCTGGTCCGCGCGGTTT
GTACCGTACACCACTGAGACCGCGGTGGTTGACCAGACAAACCCGCGCCCCGCACGATCAGACGGTCGGCCACC
GGTCTCCTTTCACACTGCCCTATGCAGGTGTTTTCGCGT

Cell culture and Infection.

Bone marrow derived macrophages (BMDMs) were differentiated from cryopreserved bone marrow stocks extracted from femurs of 8-week-old C57BL/6 mice. After cultivation for 7 days in Petri dishes in BMDM differentiation medium (DMEM with 10% FBS, 1% sodium-pyruvate, 1% GlutaMax and 20% L929-cell-conditioned medium as a source of granulocyte/macrophage colony stimulating factor) adherent cells were gently lifted from the plate using a cell scraper, resuspended in BMDM culture medium (DMEM with 5% FBS, 1% sodium-pyruvate, 1% GlutaMax and 5% L929-cell-conditioned medium) and seeded on the plate used for the the experiment. For infection, 1 ml of *M. smegmatis* or *M. abscessus* culture at OD_{600} 0.4-0.8 was pelleted, resuspended in 200 µl of BMDM culture medium and passed through a 5 µm filter to eliminate bacterial aggregates. The resulting single-cell suspension was used to infect BMDMs at an MOI of 1:1. After 4 hours of infection, macrophages were washed extensively to remove extracellular bacteria and incubated with fresh macrophage medium. All the incubations were performed at 37°C, 5% CO_2. When required, 100 U/ml IFNγ was added to the macrophage medium 16 hours before infection and kept during the experiment. At selected time-points post infection macrophages were lysed with 0.5% Triton X-100 in PBS for 5 minutes to collect the intracellular bacteria. The cell lysate was pelleted, washed twice with PBS and the pellet was resuspended in 7H9 for further microscope imaging.

RAW264.7 macrophages were infected with *M. abscessus* or *M. smegmatis* (MOI 10:1) for 30 minutes before washing cells and adding gentamicin (50 µg/ml) for 1 hour to remove extracellular bacilli. When required, IFNγ (100 U/ml) was added to macrophages 12 hours prior to infection and kept during the experiment. At 48 hours of infection, macrophages were thoroughly washed with fresh medium and lysed with 0.5% Triton X-100 in PBS for 5 minutes to collect intracellular bacilli. The cell lysate was pelleted, washed twice with PBS to remove detergent, and samples either serial diluted to plate for CFU or loaded onto standard isotonic Percoll to fractionate differentially buoyant bacilli by buoyancy gradient centrifugation.

Optical Fluorescence Microscopy.

Bacteria extracted from macrophages were seeded on a 35 mm Ibidi µ-dish and imaged for up to 24 hours at 1-hour intervals to check for growth recovery. Infected BMDMs were imaged for up to 72 hours at 1-hour intervals. All the microscopy images were acquired on a DeltaVision microscope equipped with an enclosure maintaining the temperature of the sample at 37°C, FITC (Ex 490/20, Em 525/36) and TRITC (Ex 555/25, Em 605/52) filters and 60x or 100x objectives. Host cells and bacteria were respectively identified in bright-field and fluorescence images. Multiple XY fields were acquired in parallel. For microscope experiments with macrophages, samples were maintained in a humidified stage-top incubator connected to a gas mixer (Okolab) supplying air mixed to 5% CO_2. For some experiments, macrophages imaged by time-lapse microscopy were lysed by replacing the macrophage medium with 0.5% Triton X-100 in PBS using custom-made tubing connected to the lid of the macrophage dish. After 5 minutes, cells were washed gently with PBS and then incubated with 7H9 medium supplemented with 100 ng ml^{-1} calcein-AM to identify live, enzymatically active cells. Bacteria sticking to the debris of the lysed cells were imaged by time-lapse microscopy to track their regrowth.

Image analysis.

The microscopy images and time-series were analysed using the FIJI software from the ImageJ package (Schindelin et al., 2012). Macrophage infection status and viability were monitored by visual analysis of the time-lapse bright-field image series. Regions of interest corresponding to individual macrophages were manually drawn onto the bright-field images and transferred to fluorescence images. A manual threshold was set on the fluorescent channel to segment the bacteria. The area above the threshold for each region of interest was measured for each time-point and used as a proxy for the number of intracellular bacteria per cell. The bacterial growth rate of each individual intracellular micro-colony was calculated fitting an exponential curve was fitted to the measured fluorescent areas. For individual bacteria extracted from lysed macrophages, regrowth and staining were manually analysed through visual inspection of the microscope image series.

AFM imaging.

Coverslips were prepared as previously described [9]. Polydimethylsiloxane (PDMS) (Sylgard 184, Dow Corning) at a ratio of 15:1 (elastomer:curing agent) and cut 1:10 with Hexane to reduce 10-fold the spin-coated layer, while equally increasing the hydrophobicity of the surface. Aliquots of mycobacteria isolated from axenic culture or from infection of macrophages were filtered thourgh a 0.5 µm pore size PVDF filter (Millipore) to remove cell clumps and enrich single cells. Aliquots were deposited on the hydrophobic surface of a PDMS-coated coverslip. 7H9 growth medium was supplied. Where indicated, antibiotic was added to the growth medium. The medium was maintained at 37°C using a custom-

made heating element within the sample space and a TC2-80-150 temperature controller (Bioscience tools). Bacteria were imaged by peak force tapping using a Nanoscope 5 controller (Veeco Metrology) at a scan rate of 0.25 – 0.5 Hz and a maximum Z-range of 5 µm. A ScanAsyst fluid cantilever (Bruker) was used. Continuous scanning provided snapshots at 2-30 min intervals. Height, peak force error, adhesion, dissipation, deformation modulus and log modulus were recorded for all scanned images. Peak force error yields a fine representation of the height on the order of 10 nm in the Z-axis; this is computed as the difference between the peak force setpoint and the actual value. Images were processed using Gwyddion (Department of Nanometrology, Czech Metrology Institute). ImageJ was used for extracting bacterial cell surface height and modulus values and generating dynamic and quantitative mean values of the mechanical properties of individual cells.

Correlated fluorescence and AFM.

Correlated fluorescence and AFM images were acquired as described previously [9,37]. Briefly, fluorescence images were acquired with an electron-multiplying charge coupled device (EMCCD) iXon Ultra 897 camera (Andor) mounted on an IX71 inverted optical microscope (Olympus) equipped with an UAPON100XOTIRF x100 oil immersion objective (Olympus) with the x2 magnifier in place. Illumination was provided by a monolithic laser combiner (MLC) (Agilent) using the 488 or 561 nm laser output coupled to an optical fibre with appropriate filter sets: F36-526 for Calcein-AM and F71-866 for mCherry-Wag31 or cytosolic RFP. The AFM was mounted on top of the inverted microscope and images were acquired with a customised Icon scan head (Bruker) using ScanAsyst fluid cantilevers (Bruker) with a nominal spring constant of 0.7 N m^{-1} in peak force tapping mode at a setpoint <2 nN and typical scan rates of 0.5 Hz. The samples were maintained at 37°C in 7H9 growth medium heated by a custom-made coverslip heating holder controlled by a TC2-80-150 temperature controller (Bioscience tools).

Cell measurements.

Fundamental physiological cell measurements of both cell dimensions and mechanical surface rigidity were made as described previously [9,11,14,18,19].

Cell growth measurements. Cell growth herein describes a process of cell expansion, which is defined as a function of both cell elongation along the long axis of the cell and surface mechanical maturation (change in cell surface stiffness) upon the addition of nascent cell wall material. Cell length was measured as per [9-11]. Mechanically distinct cell growth zones were segregated into three spatially discrete zones based on the dynamic and mechanical state of the surface: 1) the nascent growth zone consists of mechanically "soft" material typically localised nearest the poles in mycobacteria, 2) a maturation zone consists of the space adjacent to the nascent zone where surface material is dynamically increasing in mechanical rigidity, and 3) a mechanically mature zone where surface material mechanical properties has ceased to increase.

Mean cell surface stiffness. Mycobacterial cell surface stiffness is averaged over the relatively flat surface along the longitudinal midline of the cell surface, which is probed by AFM imaging in peak force tapping mode and interpreted as the Young's modulus as per the Derjaguin-Muller-Toporov (DMT) model. The absolute values can vary from one experiment to the next, as a function of variations in the biophysical properties of the fluid medium (temperature and fluid density). Therefore, the mean cell

surface rigidity is interpreted as a relative measure comparing the bacterium to the modulus of the PDMS-coated coverslip sample surface (Supplementary Figure 14).

Buoyant density. Buoyancy fractionation was conducted by centrifuging mycobacteria at high speeds in a viscous, gradient-forming medium. Stock isotonic percoll medium (SIP) is prepared by mixing 9ml Percoll with 1ml 0.15 M NaCl. 10 ml of SIP was loaded into thin wall polypropylene centrifuge tubes (14 x 89 mm) (Beckman Coulter) along with 1 ml of bacterial sample and 50 µl of buoyancy centrifuge beads. Mycobacteria are centrifuged at 20,000 rpm (~52,000 g) for 1 hour and 20 minutes using a Beckman Coulter Optima L-90K Ultracentrifuge and a SW40Ti swinging bucket rotor. Buoyant density beads (Cospheric) at 1.02 g cm^{-3}, 1.064 g cm^{-3}, 1.08 g cm^{-3}, and 1.102 g cm^{-3} were used to distinguish "high", "middle" and "low"-buoyancy fractions of mycobacteria.

Reporting Summary.

Information regarding the experimental design is available in the *Nature Research Reporting Summary*.

Data availability.

Tnseq raw datasets are available at : https://figshare.com/s/221d724865faa6deb7e4. Select LTTL-AFM datasets are available at : https://figshare.com/s/4a63d8e2186f8246077d. Raw experimental data supporting the findings of these studies are available from the corresponding author upon request.

585 **Figure Legends:**

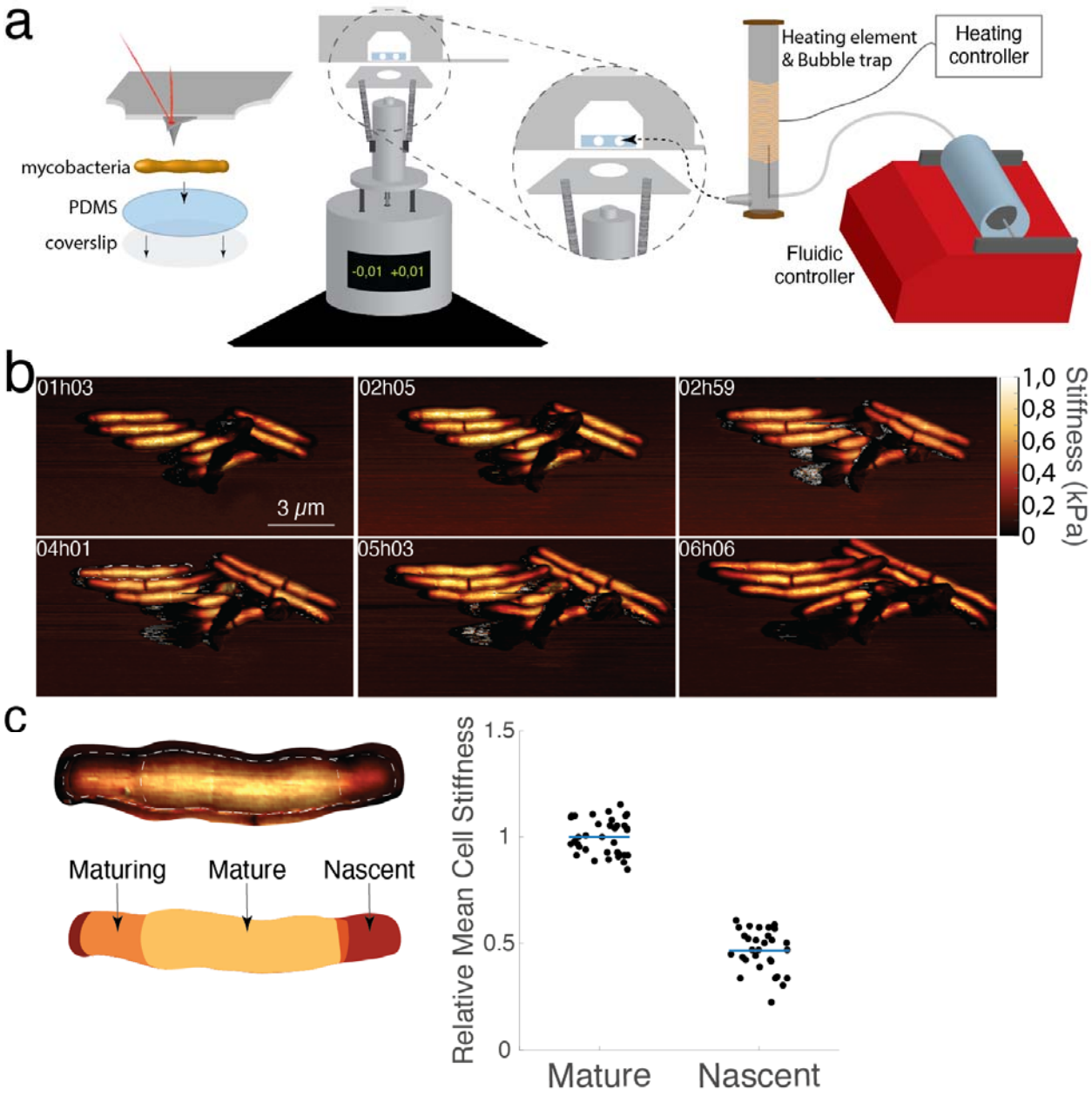

586
587 **Figure 1. The mycobacterial cell wall controls surface mechanical maturation.**
588 **a**, Schematic representation of the LTTL-AFM imaging system depicting the setup for mycobacterial
589 sample scanning (left) and the integrated heating element and fluidic systems (right) for controlling the
590 environmental conditions while scanning with a Bruker MultiMode 8. **b**, Time series of three-
591 dimensional AFM height images overlaid with mechanical stiffness (DMT modulus) images for wilde-
592 type *M. smegmatis*. **c**, The relative cell surface stiffness of nascent cell wall material as compared to
593 mature material. n = 30.
594
595

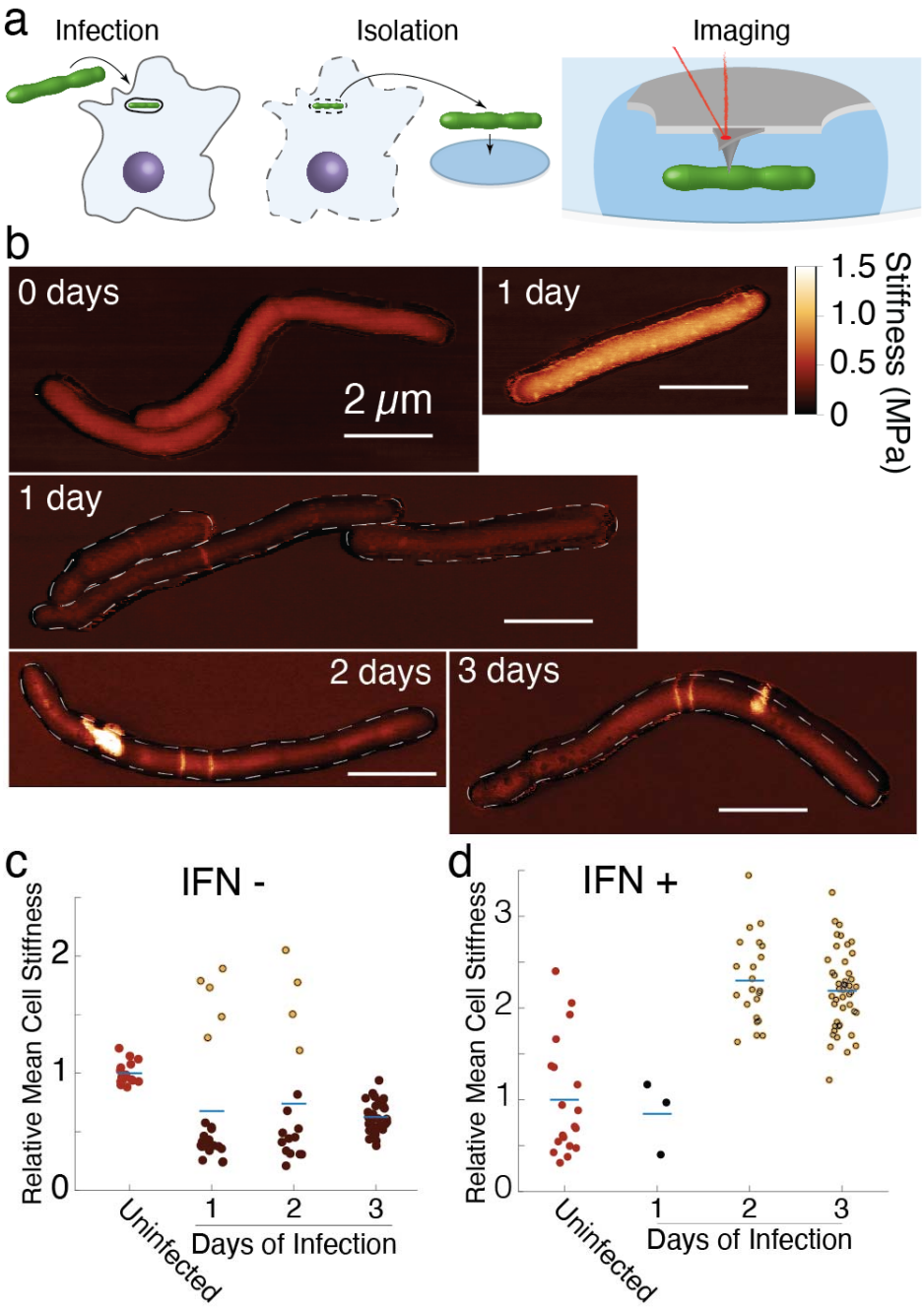

Figure 2. Host macrophage internalisation drives mycobacterial mechanical adaptation. **a**, Schematic representation of three critical steps for quantifying surface mechanical properties of macrophage-intracellular mycobacterial cells. **b & c**, Three-dimensional AFM height images overlaid with stiffness (DMT modulus) images of mycobacterial cells isolated from macrophages during a three-day infection time-course. Normalised relative mean mycobacterial cell stiffness compared to the mean cell stiffness of intracellular mycobacterial cells isolated from macrophages altogether showing the emergence of mechanically "hard" and "soft" cell morphotypes during infection. **d**, Mycobacteria isolated from macrophages treated with interferon-gamma all exhibited a relative increase in cell surface stiffness. Bar represents mean and dots measurements from individual bacilli.

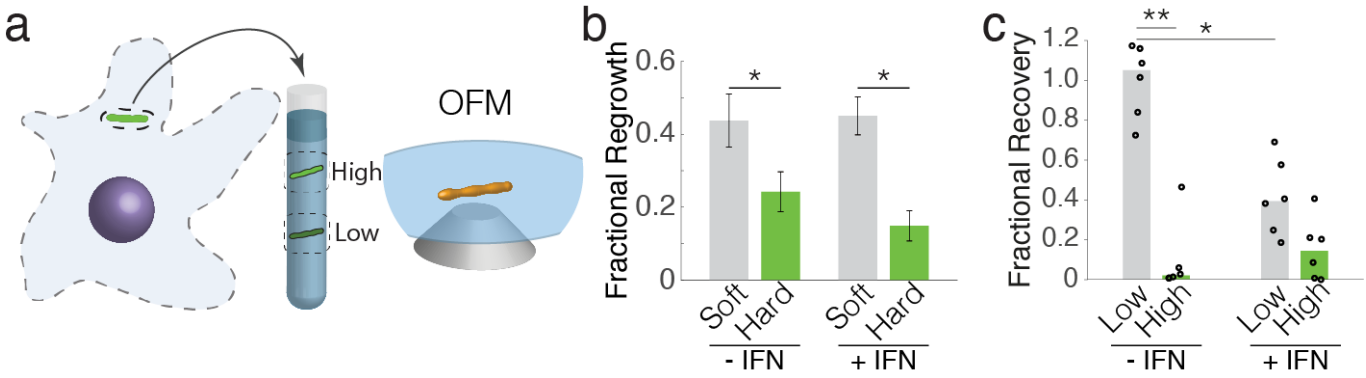

Figure 3. Fractional recovery and regrowth of mechanical morphotypes.

a, Schematic representation of the process by which mechanical morphotypes are isolated from macrophages and enriched by buoyancy fractionation. Enriched mycobacterial morphotypes were analysed for their fractional recovery by quantifying the rate of regrowth using optical fluorescence microscopy (b) and by colony forming units (cfu) (c). **b**, 100 mycobacteria were randomly selected and tracked for 48 hours to quantify whether regrowth would take place. Bars represent the fraction of individuals undergoing regrowth +/- standard error of the mean from three biological replicates (SEM). The "soft" mechanical morphotype exhibited increased regrowth versus the "hard" when isolated from macrophages, independent of cytokine-stimulation. **c**, Fractional recovery as measured by cfu represents values corrected for the number of mycobacteria isolated from macrophages in each sample, showing that cytokine stimulation reduces the yield of sample. *$P < 0.05$, **$P < 0.01$.

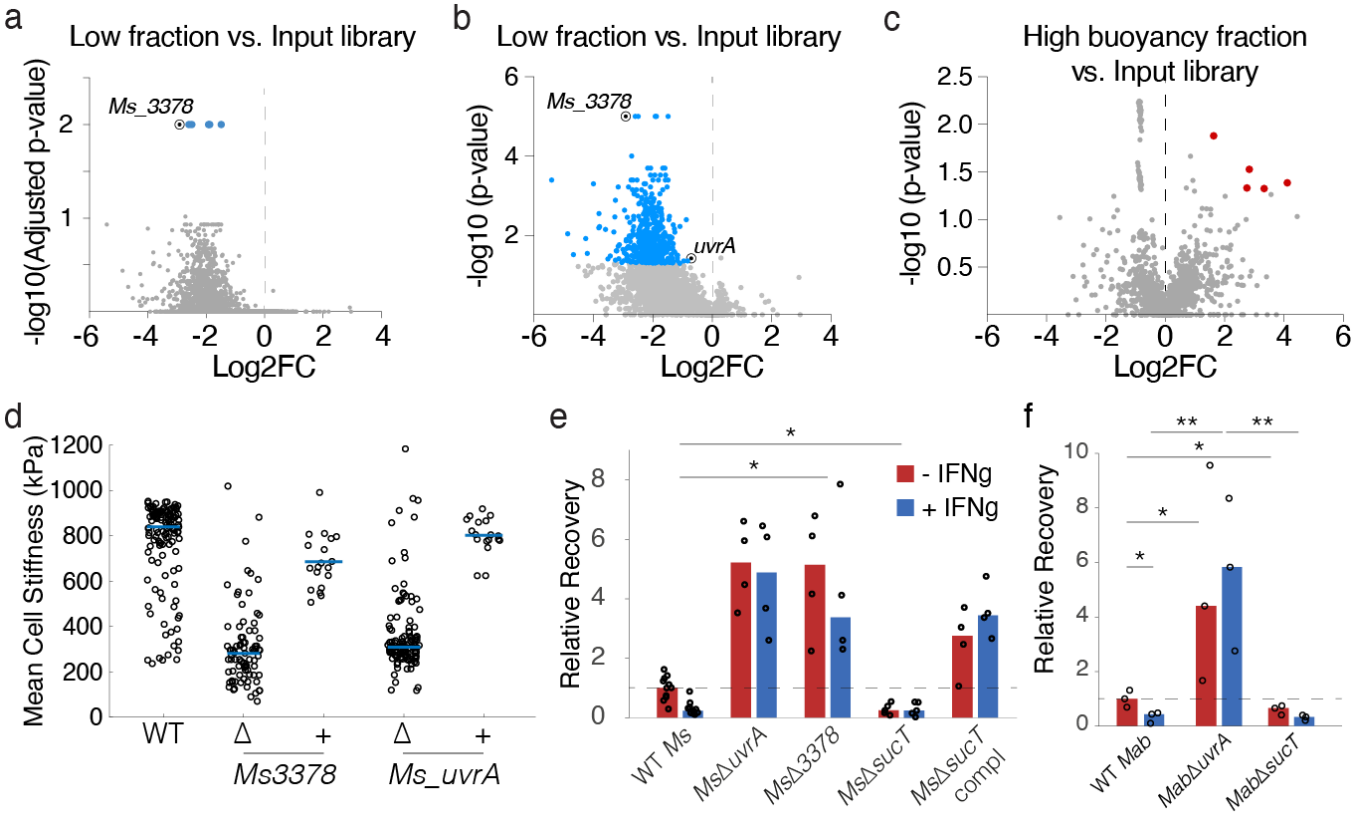

Figure 4. "Soft" mechanical morphotype mutants enhance macrophage infection.
Volcano plot of genes with different transposon insertions against adjusted p-value (**a**) or p-value (**b**) by re-sampling test for TnSeq analysis of low fraction vs. input library and high fraction vs. input libraries (**c**), genes with differential transposon insertions (see method) are marked in blue and red dots. **d**, Mean cell surface stiffness, quantified using AFM, of wildtype *M. smegmatis* and "soft" mechano-morphotype mutant strains. **e & f**, Relative recovery of mechanical morphotype mutants in *M. smegmatis* (**e**) and *M. abscessus* (**f**) following 48-hour infection in macrophages untreated or treated with IFNγ. Bars represent mean +/- SEM. **P* < 0.05, ***P* < 0.01.

633 **Supplementary Figures :**
634

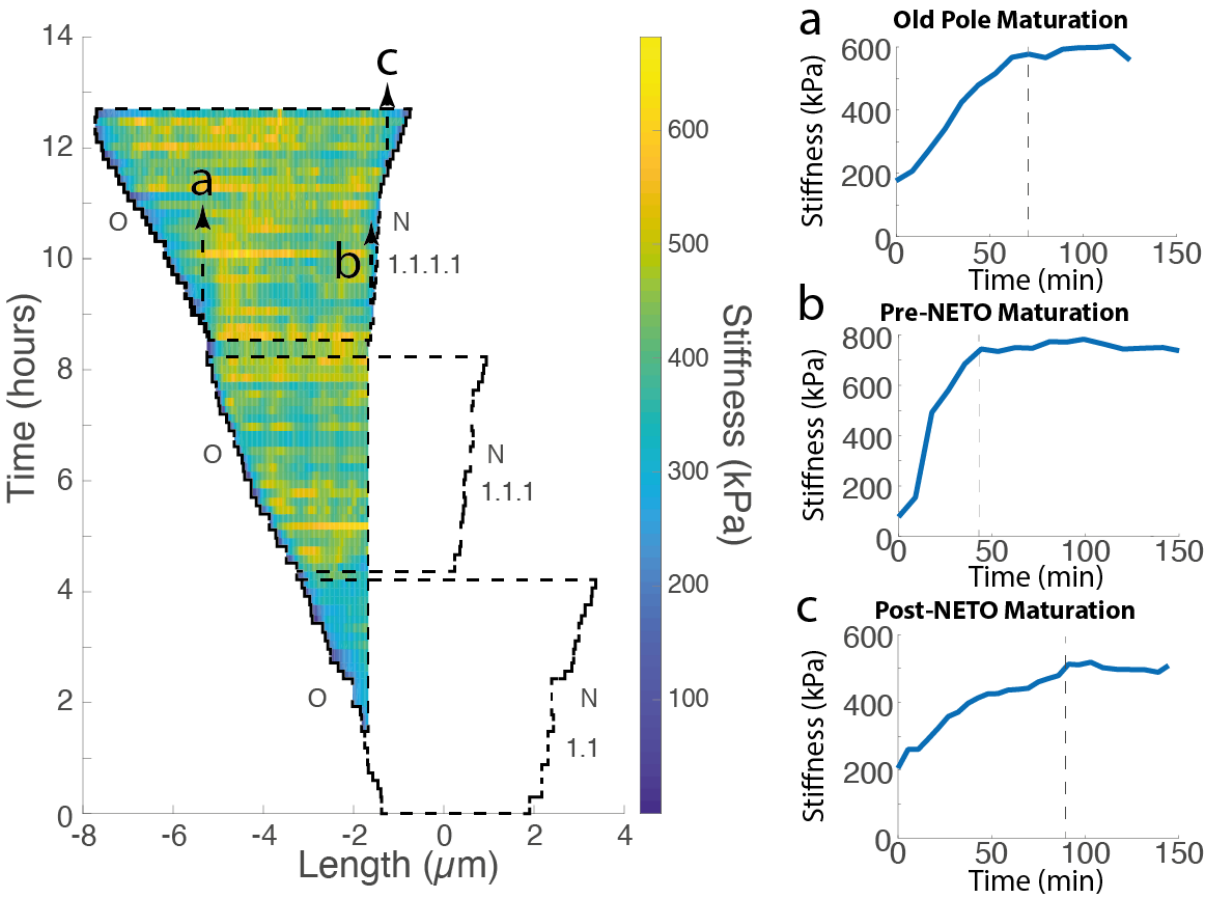

635
636 **Supplementary Figure 1. Mycobacterial cell surface mechanical growth dynamics.**
637 Kymograph representation of the cell surface of *M. smegmatis* over three successive generations of
638 growth and division. Depicted is the spatial inheritance of cell surface material from when it is first
639 deposited as a result of polar elongation. **a – c**, The dynamic of "mechanical maturation" of nascent
640 material increases in surface stiffness until it plateaus. The rate of maturation is distinguishable
641 depending on the age of the pole and the timing of "new-end take-off" at the new pole [10]. The spatial
642 mobility of mechanically mature material is static, as is equally reported for chemically distinct layers [38].
643
644

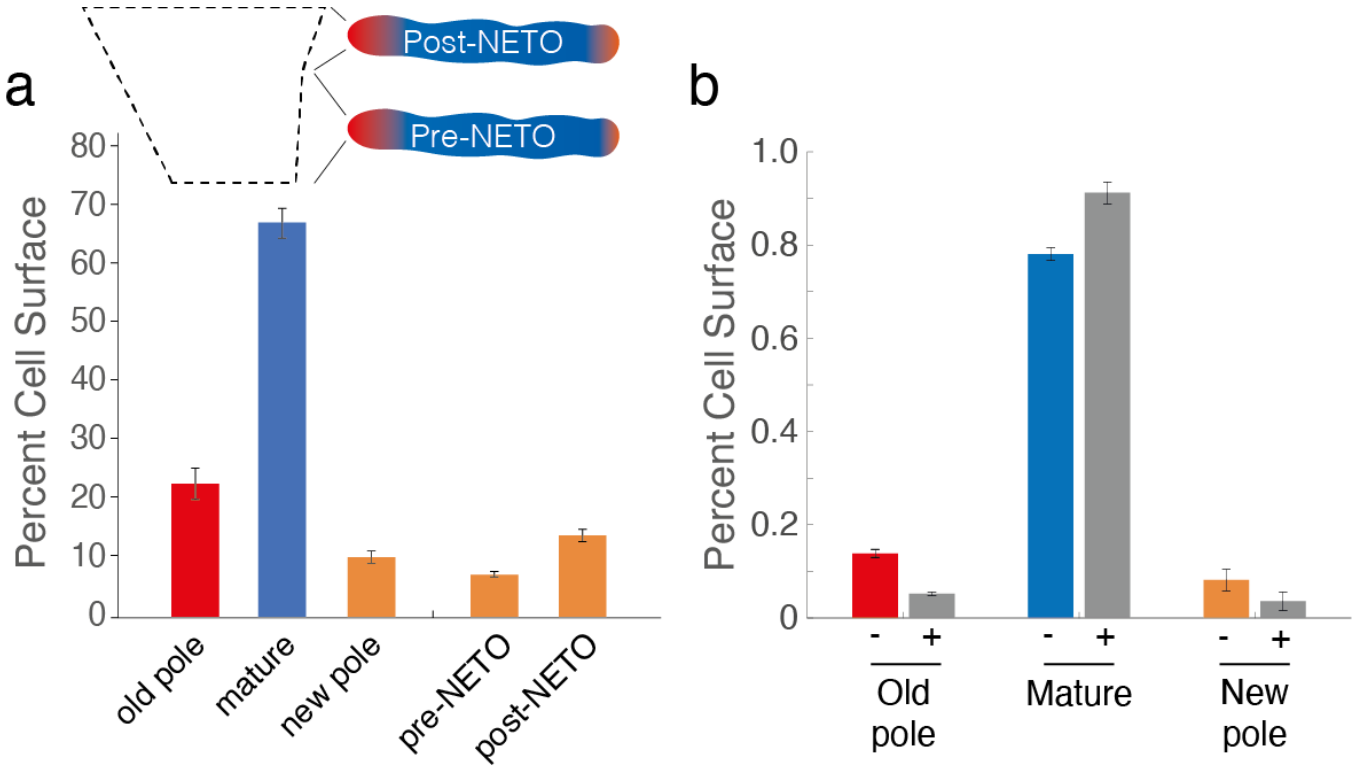

Supplementary Figure 2. The spatial percentage of the cell surface of *M. smegmatis* as measured by LTTL-AFM quantitative nanomechanical mapping. (a) In growing *M. smegmatis* in axenic conditions of growth, mechanically stable cell surface material represents >60% of the cell surface (blue bar). Cell surface material that is actively undergoing an increase in mechanical rigidity represents ~30% of the cell surface split between the old and new poles (red and orange bars). The spatial representation of new pole material can be distinguished as a function of whether new-end take-off (NETO) has taken place [10]. (b) Concomitant with cessation of elongation, INH-treated bacilli (grey bars) exhibit decreased spatial distributions of mechanically nascent cell surface material at each of the cell poles. Bars represent mean +/- SEM.

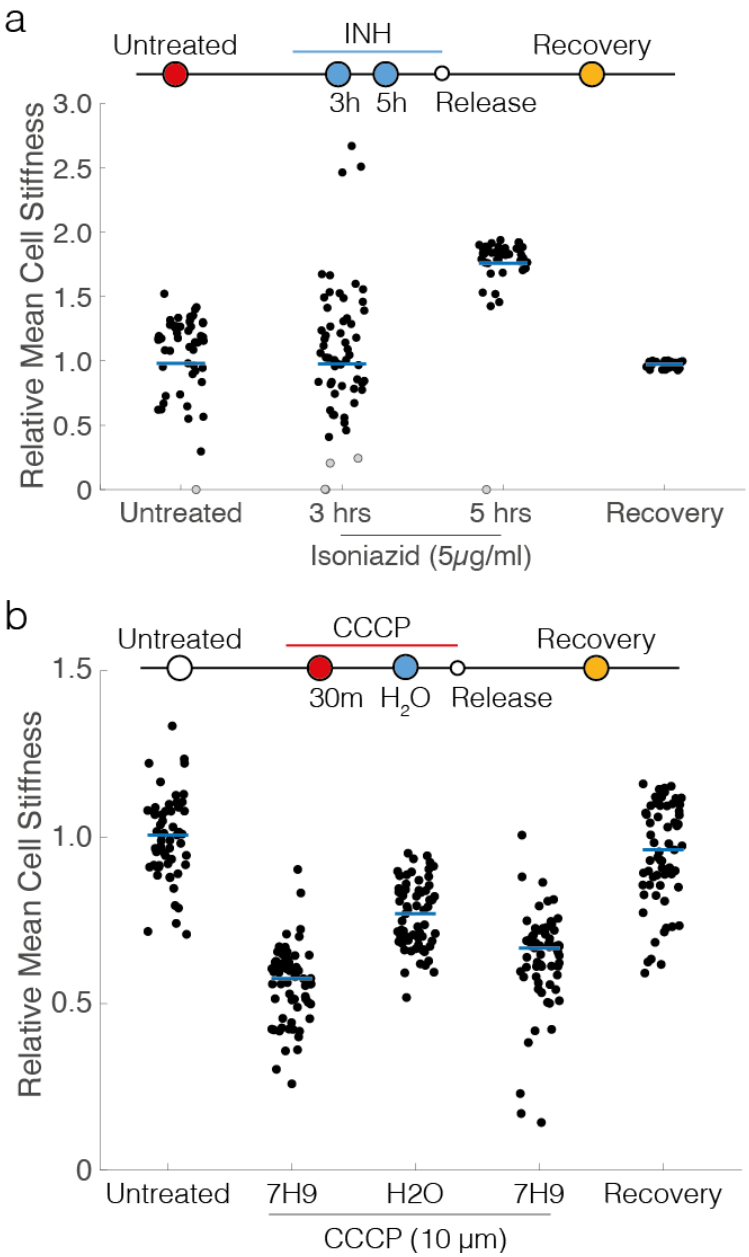

Supplementary Figure 3. Relative mean cell surface stiffness of antibiotic-treated *M. smegmatis*. *M. smegmatis* treated with INH (5 μg/ml) (a) or CCCP (10 μM) (b). Bacilli treated with CCCP was probed within 30 minutes; CCCP-treated bacilli were subsequently exposed to osmotic shock by transiently exchanging growth medium (7H9) with dH_2O, before adding back 7H9 with CCCP, before later releasing bacilli from CCCP-treatment. Recovery represents the mean cell surface stiffness of cells surviving antibiotic treatment, which undergo regrowth and culminate in division, at which point the cell stiffness is probed. The relative mean cell surface stiffness represents a comparison of the mean cell surface stiffness for INH-treated cells to untreated cells. Black dots represent living cells (a & b). Grey dots represent dead cells (a).

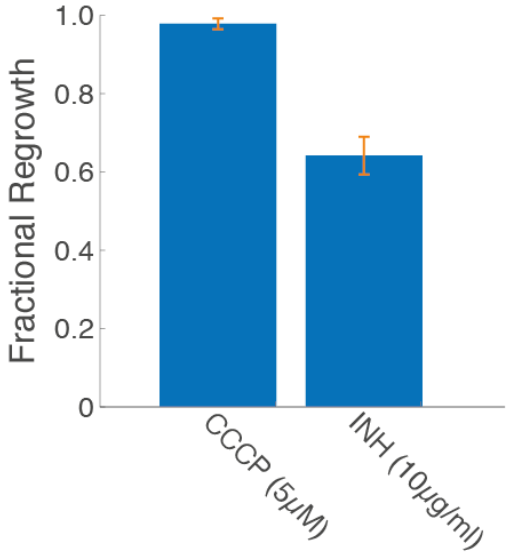

Supplementary Figure 4. Fractional recovery of *M. smegmatis* released from antibiotic treatment.
M. smegmatis bacilli, released from antibiotic treatment during LTTL-AFM imaging at 37°C, are counted for their ability to regrow among all surviving bacteria. Bars represent mean +/- SEM.

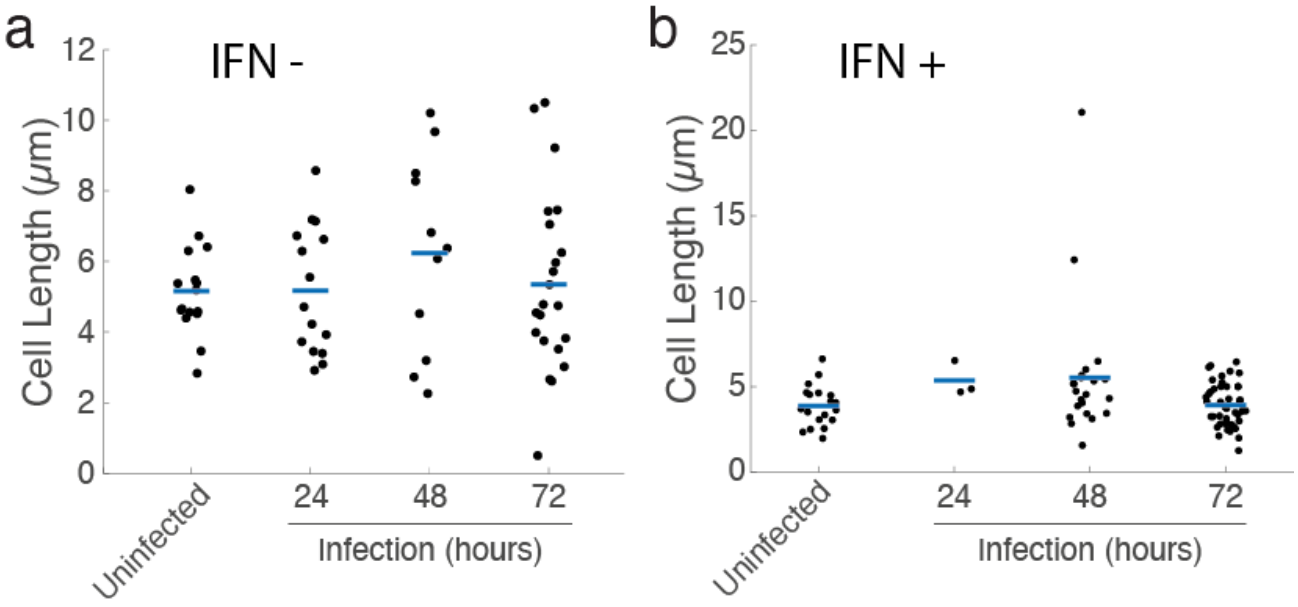

Supplementary Figure 5. Mycobacterial cell length heterogeneity.
The length of *M. smegmatis* cells is isolated measured by AFM at room temperature (25°C) to probe the mechanical properties in static conditions. Mycobacteria were isolated from macrophages (-/+ IFNγ) and resuspended in 7H9. Blue bars represent the mean of each sample distribution.

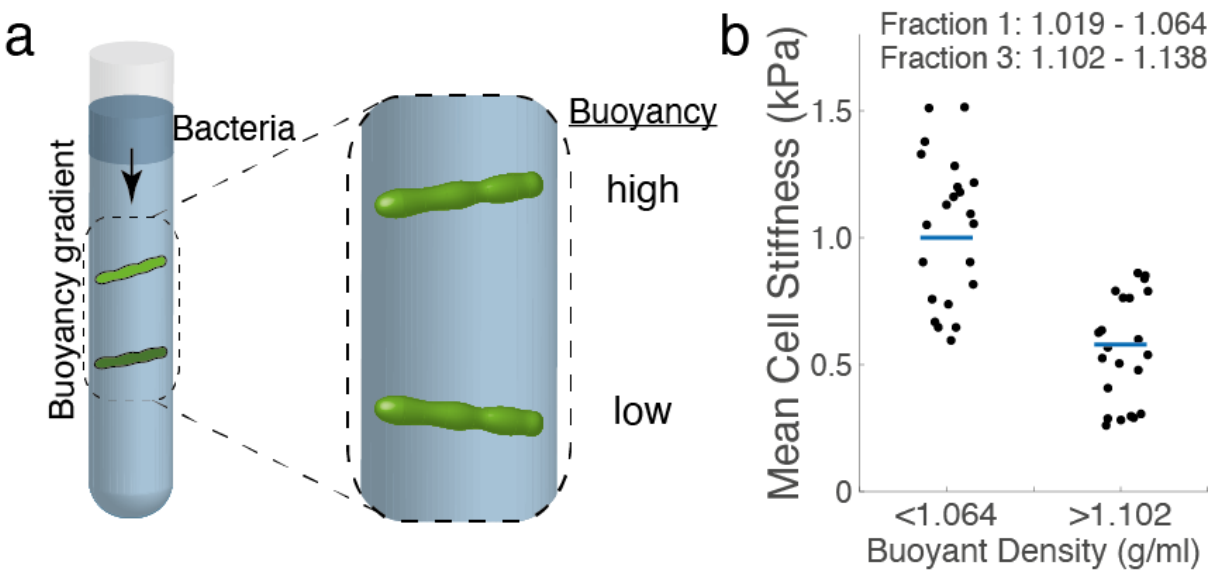

Supplementary Figure 6. Buoyancy centrifugation as a surrogate measure for cell surface stiffness measured by AFM.

a, Schematic representation of buoyant density centrifugation to fractionate high and low buoyancy mycobacteria through stock isotonic Percoll (SIP). The enrichment process consists of three successive rounds of buoyancy centrifugation followed by regrowth of high and low buoyancy fractions in permissive growth medium. **b,** AFM stiffness measurements of mycobacteria isolated from high (< 1.064 g/ml) and low (> 1.102 g/ml) buoyancy fractions. Blue bars represent mean. Black dots represent individual bacilli of *M. smegmatis*.

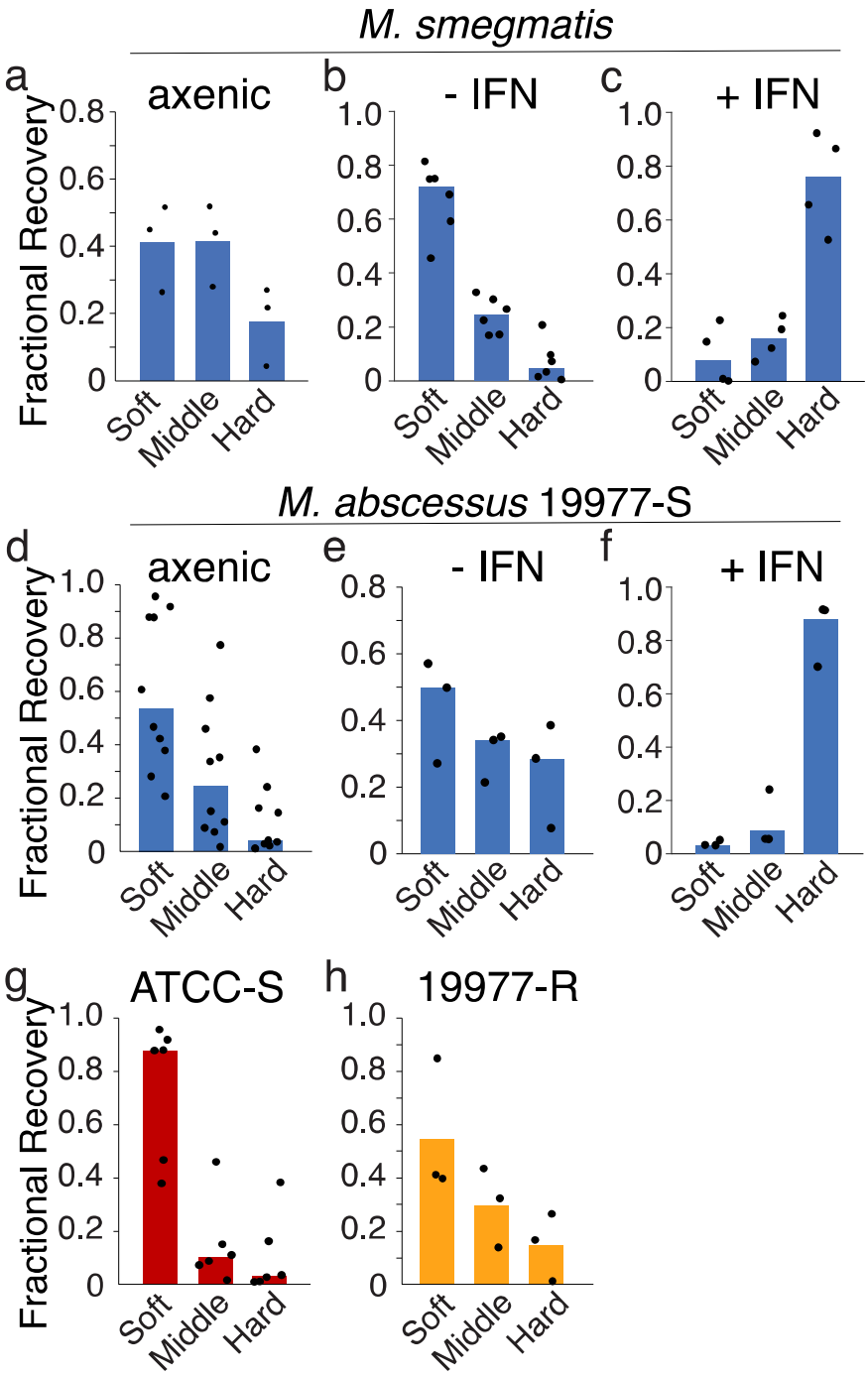

Supplementary Figure 7. Distribution of buoyancy of mycobacteria.
M. smegmatis **(a – c)** and *M. abscessus* strain 19977 (smooth morphotype) **(d – f)** fractionated following culturing in 7H9 growth medium (a & d) or isolated from macrophages untreated (b & e) or IFNγ-treated (c & f). Fractionation of *M. abscessus* strain ATCC (smooth morphotype) **(g)** and strain 19977 (rough morphotype) **(h)** grown in 7H9 growth medium. *M. abscessus* 19977-R represents a rough colony morphotype whereas 19977-S and ATCC-S both represent smooth colony morphotype strains. Bars represent mean and dots represent individual experimental replicates.

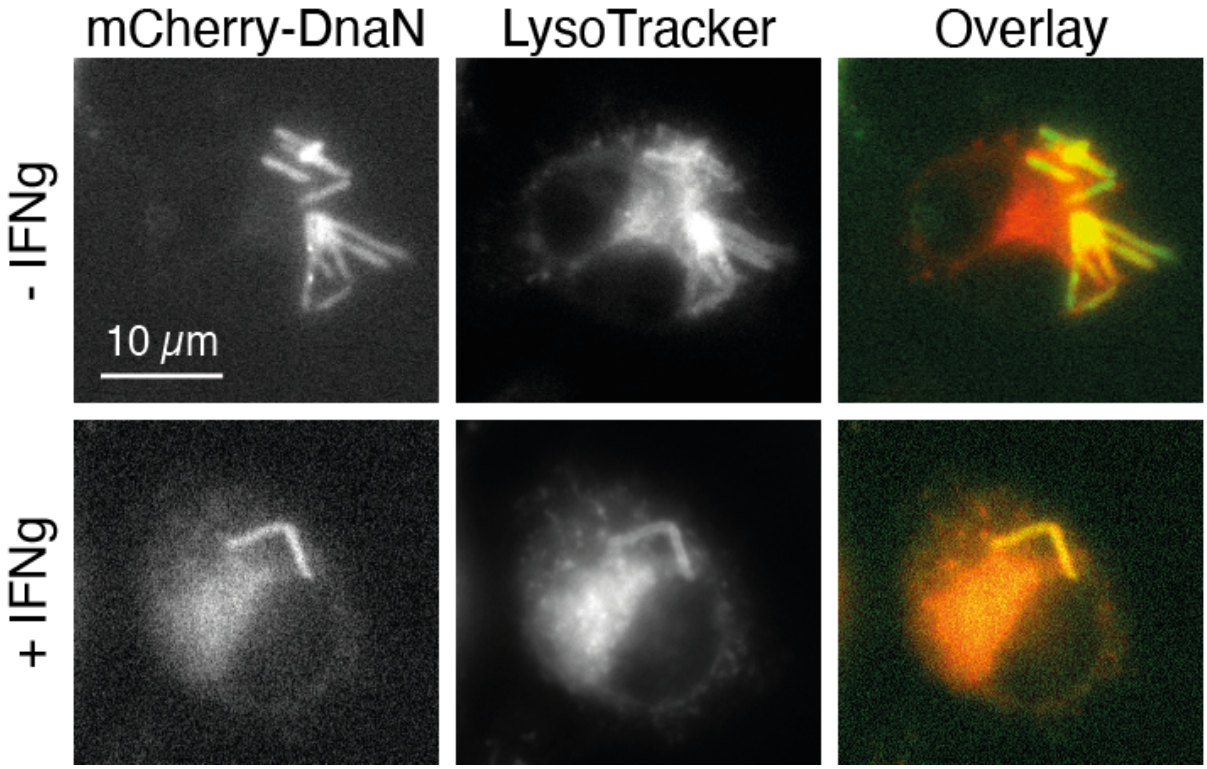

Supplementary Figure 8. Acidification of *Mycobacterium*-containing vacuoles. Optical fluorescence imaging of macrophages -/+ IFNγ harboring *M. smegmatis* expressing mCherry-tagged DnaN (integrated at the *attB* locus) [39]. Macrophages stained with lysotracker reveal the state of acidification of vacuoles harboring *M. smegmatis* in both unstimulated and cytokine-stimulated macrophages.

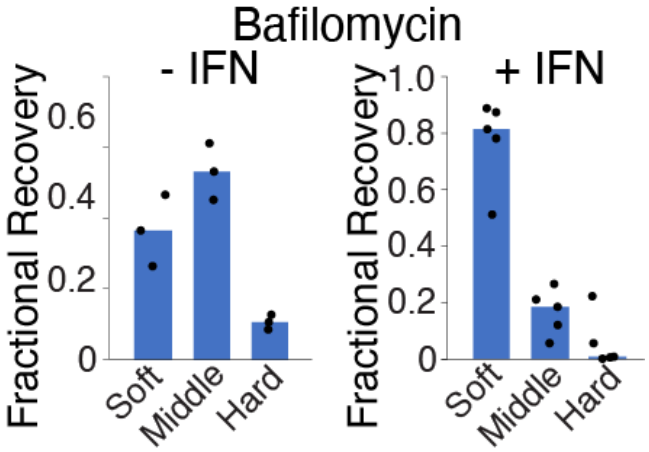

Supplementary Figure 9. Vacuolar acidification is necessary for the selection of "high" buoyancy *M. smegmatis* in IFNγ-stimulated macrophages. Fractional recovery of *M. smegmatis* following buoyancy centrifugation after bacilli were isolated from -/+ IFNγ-treated macrophages equally treated with Bafilomycin A (10 μM, added at infection start). Bars represent mean and dots represent individual experimental replicates.

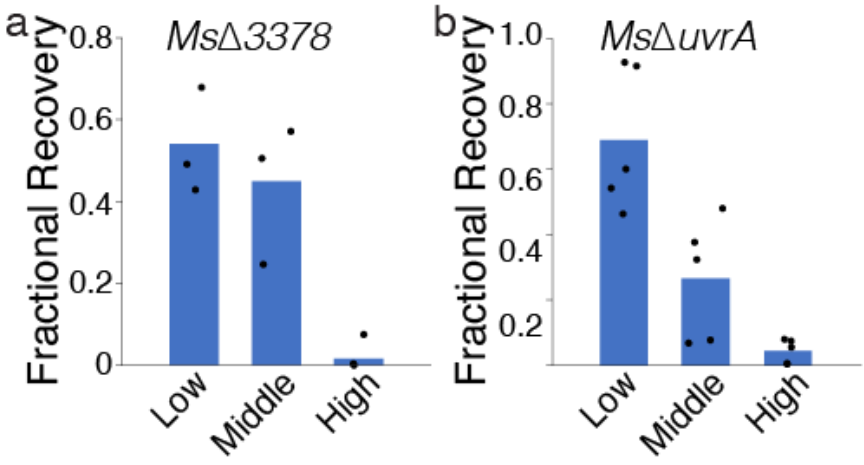

Supplementary Figure 10. Fractional recovery of buoyancy fractionated "soft" mechanical morphotype mutants cultured in axenic conditions of growth. Bars represent mean and dots represent individual experimental replicates.

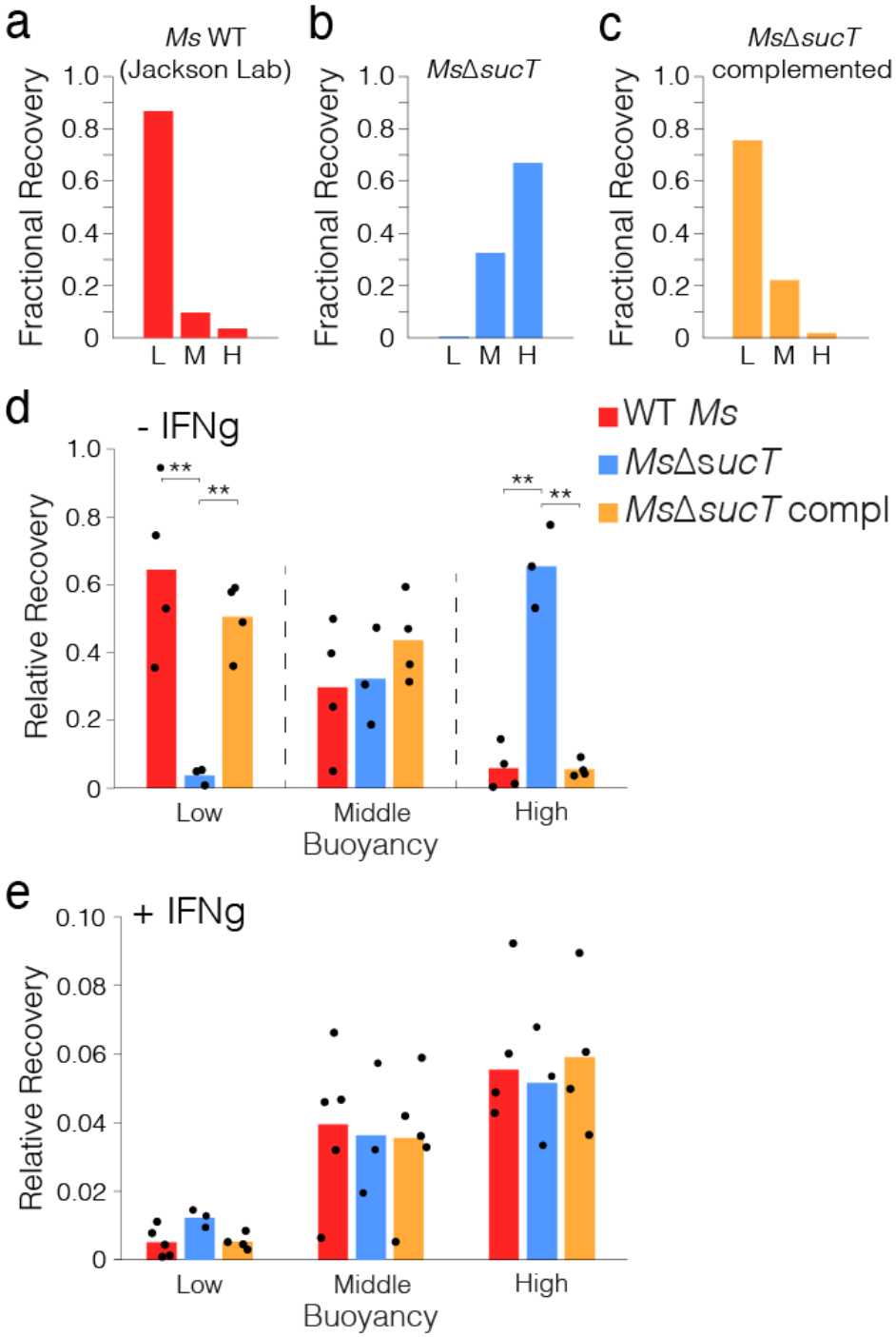

Supplementary Figure 11. Relative fractional recovery of *M. smegmatis* Δ*sucT*. a-c, The fractional recovery of *M. smegmatis* wildtype, Δ*sucT*, and complemented *sucT* cultured in axenic conditions of growth. **d** & **e**, Relative fractional recovery of mycobacterial strains isolated from macrophages and buoyancy fractionated. Relative fractional recovery equally shows the relative recovery of samples from macrophages. Bars represent mean and dots represent individual experimental replicates.

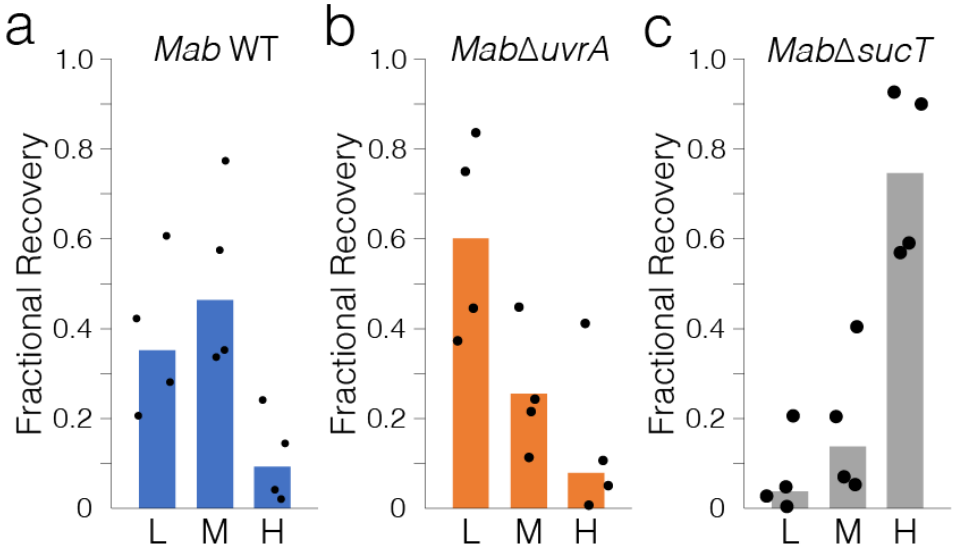

Supplementary Figure 12. Fractional recovery of *M. abscessus* mechanical morphotype mutant candidates buoyancy fractionated following culturing in axenic conditions of growth. Bars represent mean and dots represent individual experimental replicates.

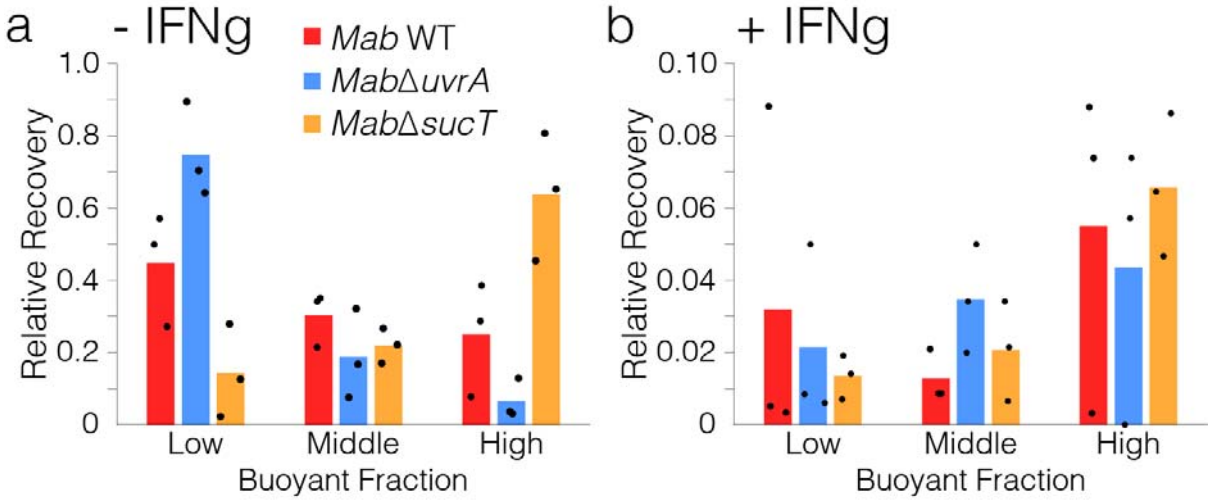

Supplementary Figure 13. Distribution in buoyancy for a "hard" mechano-morphotype mutant candidate. Bars represent mean and dots represent individual experimental replicates.

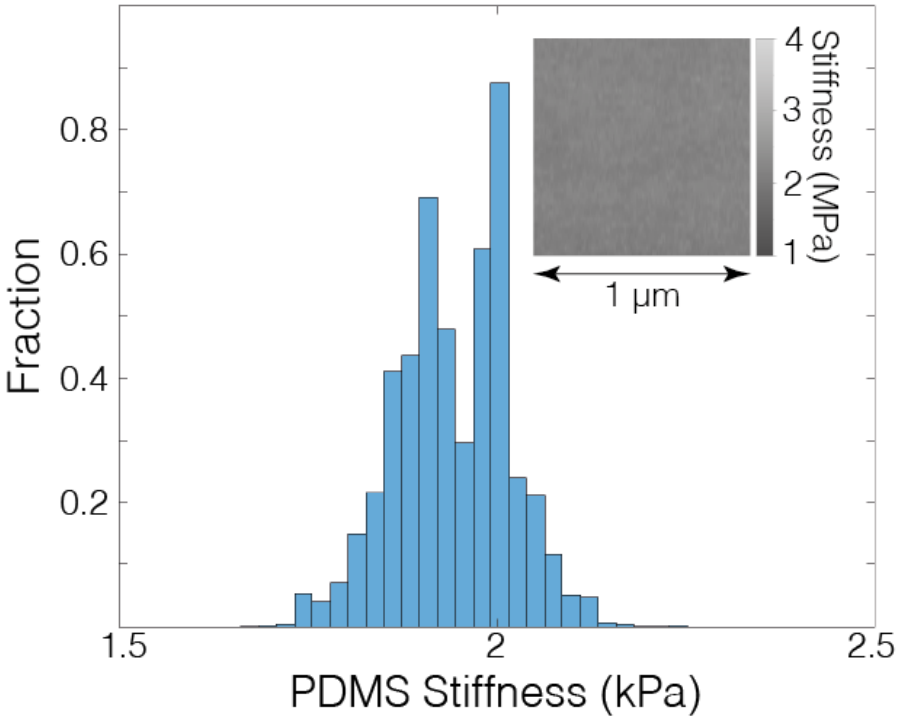

Supplementary Figure 14. Calibrating AFM stiffness measurements from DMT modulus images was conducted using the polydimethylsiloxane-coated coverslip sample surface with known Young's modulus of ~1.8 MPa. Histogram depicts the distribution of measurements. Inset AFM DMT modulus image represents the measurements made using the AFM imaging mode: peak force quantitative nanomechanical mapping.

Supplementary Videos :

Supplementary Video 1. LTTL-AFM imaging of *M. smegmatis* cultured in axenic conditions of growth. AFM imaging was conducted using peak-force off-resonance tapping in time lapse. 3D-Height images are overlayed with the DMT Modulus. *M. smegmatis* was grown at 37°C and the frequency of images taken every 9 minutes. Images represent 15 µm by 7.5 µm of space. The scale of DMT modulus spans 0 – 3 MPa. See Figure 1b and Supplementary Figure 16 for representative schematic images of the same time-lapse.

Supplementary Video 2. LTTL-AFM imaging of *M. smegmatis* Δ*ldtAEBCG+F* cultured in axenic conditions of growth. AFM DMT modulus images depicting the cell surface stiffness of a mycobacterial mutant in which all L, D Transpeptidases are absent resulting in less peptidoglycan crosslinking at the new pole defective. The mechanical consequence is bulging spatially localised near the new pole, which happens at a rate that is controlled by the addition of new material at the cell wall [14].

Supplementary Video 3. LTTL-AFM imagine of *M. smegmatis* WT cells cultured in axenic conditions of growth and antibiotic stress. AFM peak force error images depict the cell surface of *M. smegmatis* cells.

Supplementary Video 4. LTTL-AFM imagine of *M. smegmatis* WT cells cultured in axenic conditions of growth and antibiotic stress as per Supplementary Video 3. AFM DMT Modulus images depict the cell surface of *M. smegmatis* cells in conditions of growth, treatment with the bacteriostatic CCCP (5 µM), and recovery of bacilli following washout of the drug.